THE JOURNAL OF PHYSICAL CHEMISTRY B

Article

pubs.acs.org/JPCB

# A Theoretical Reappraisal of Polylysine in the Investigation of Secondary Structure Sensitivity of Infrared Spectra

Laura Zanetti Polzi,[†] Isabella Daidone,*[,†] and Andrea Amadei*[,‡]

[†]Department of Chemistry, Chemical Engineering and Materials, University of L'Aquila, via Vetoio (Coppito 1), 67010 L'Aquila, Italy

[‡]Department of Chemical Sciences and Technology, University of Rome "Tor Vergata", via della Ricerca Scientifica 1, 00133 Rome, Italy

**ABSTRACT:** Infrared spectroscopy has long provided a means to estimate the secondary structure of proteins and peptides. In particular, the vibrational spectra of the amide I′ band have been widely used for this purpose as the frequency positions of the amide I′ bands are related to the presence of specific secondary structures. Here, we calculate the amide I′ IR spectra of polylysine in aqueous solution in its three secondary structure states, i.e., $\alpha$-helix, $\beta$-sheet, and random coil, by means of a mixed quantum mechanics/molecular dynamics (QM/MD) theoretical−computational methodology based on the perturbed matrix method (PMM). The computed spectra show a good agreement with the experimental ones. Although our calculations confirm the importance of the excitonic coupling in reproducing important spectral features (e.g., the width of the absorption band), the frequency shift due to secondary-structure changes is also well reproduced without the inclusion of the excitonic coupling, pointing to a role played by the local environment. Concerning the $\beta$-conformation spectrum, which is characterized by a double-peak amide I′ band due to excitonic coupling, our results indicate that it does not correspond to a generic antiparallel $\beta$-sheet (e.g., of the typical size present in native proteins) but is rather representative of extended $\beta$-structures, which are common in $\beta$-aggregates. Moreover, we also show that the solvent has a crucial role in the shape determination of the $\beta$-conformation amide I′ band and in particular in the disappearance of the high-frequency secondary peak in the case of small sheets (e.g., 6-stranded).

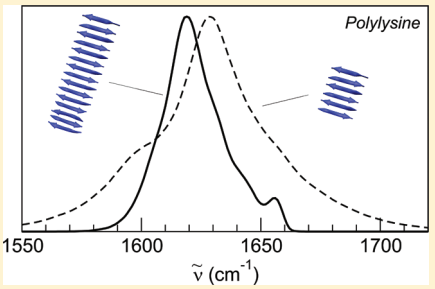


## INTRODUCTION

Infrared (IR) spectroscopy has been widely used over the past years to study the structure of peptides and proteins, as it can be used to probe changes in the secondary structure content. In particular, the IR absorption spectra of the amide I mode, mostly corresponding to the peptide-group C=O stretching, are commonly used as marker modes of secondary structure. Indeed, the frequency position of the amide I bands has been empirically related to the presence of specific secondary structures.[1−3] Nevertheless, the assignment of the amide I bands to different types of secondary structure is still a critical step in the interpretation of IR spectra of proteins. For example, amide I peaks of $\alpha$-helical structures and of disordered configurations are very close in frequency and often indistinguishable due to broadening effects.[4]

Amide I bands of $\beta$-structures are the most difficult to interpret mainly because of the various $\beta$-arrangements that can be found; one would like to distinguish between parallel and antiparallel $\beta$-sheets, $\beta$-hairpins and $\beta$-turns, $\beta$-hairpins and extended sheets, and $\beta$-sheets and $\beta$-aggregates. Some rules of thumb have been given in order to interpret $\beta$-sheets infrared spectra:[3] (i) Antiparallel $\beta$-sheets exhibit a strong band near 1630 cm$^{-1}$ and a weaker band near 1685 cm$^{-1}$; sheets with a larger number of strands have a lower spectral position of the main band. (ii) Parallel $\beta$-sheets have the main absorption at higher wavenumber than the corresponding antiparallel $\beta$-sheets, exhibit a smaller splitting between the main and sideband, and the high-wavenumber sideband is less intense. (iii) Aggregated proteins often show a band near or below 1620 cm$^{-1}$ which is characteristic of intermolecular $\beta$-sheets.

The assignment of a frequency range to $\beta$-turns and $\beta$-hairpins is more controversial. $\beta$-Hairpins are expected to show a main band in the frequency range of 1635−1645 cm$^{-1}$[5] and a high-frequency component resulting in a shoulder,[5,6] but lower frequency regions have been also assigned to the hairpin main absorption band.[7] Turn structures likely contribute to the signals near 1670 cm$^{-1}$,[3,8] but in these cases, too, also lower frequencies have been assigned to the same structure.[7]

Theoretical and computational methods are widely used to investigate the relationship between frequency range of absorption and secondary structure, and many approaches have been proposed to model protein and peptide IR spectroscopic behavior aiding in the interpretation of the experimental spectra. Rigorous *ab initio* methods for the determination of the vibrational frequencies do not allow to scale up to biologically relevant biomolecules and to properly include the complexity of the solute−solvent interplay, which would require the construction and diagonalization of the solute−solvent Hessian matrix of the quantum vibrational degrees of freedom at each representative liquid-state

**Received:** November 16, 2011
**Revised:** February 2, 2012

   dx.doi.org/10.1021/jp211063x | *J. Phys. Chem. B* XXXX, XXX, XXX−XXX

configuration. Therefore, hybrid approaches are commonly used to reproduce the band positions and line shapes of structurally well-defined molecules.[5,9−22]

Many of these[5,13−19] employ quantum mechanical (QM) calculations to determine the vibrational frequencies and eigenstates for single amides which are, then, transferred to the full peptides and/or proteins and coupled empirically. An alternative approach[20−22] makes use of Hessian calculations on the whole isolated peptide/protein in a given configuration which are, then, used to reconstruct the local, single-residue, vibrational frequencies via the Hessian matrix reconstruction method.[20] In these approaches coupling effects are included by adding a simplified electrostatic interaction, typically based on dipole−dipole interactions and commonly termed transition dipole coupling, TDC (coupling through space), and an empirical term providing the frequency variations due to first neighbors relative rotations (coupling through chemical bonds). TDC, or more generally the excitonic coupling, is considered the fundamental mechanism that renders the amide I vibration sensitive to secondary structure,[3] and for $\beta$-structures it results in the already mentioned splitting of the amide I band.

One of the most striking results emerging from a number of the above-mentioned studies[14,17,22] is that the often used empirical secondary-structure/frequency correlations are at best approximated and at worst misleading. Peptide models with a known secondary structure are used, both in experimental and in theoretical studies, to obtain information about the relationship between IR spectra and spatial arrangement. In particular, polylysine has proven to be a useful model for proteins in many studies,[4,23−25] as it can be induced to adopt the $\alpha$-helix, the $\beta$-sheet, and the random coil conformation depending on pH and temperature. The resulting IR spectra in $D_2O$ are characterized by amide I′ (i.e., the amide I in $D_2O$) maxima at ≈1645 $cm^{-1}$ for the random coil structure, ≈1635 $cm^{-1}$ for the $\alpha$-helix structure, and a main band at ≈1610 $cm^{-1}$ coupled to a weaker band at ≈1680 $cm^{-1}$ for the $\beta$-sheet structure.

Here, we calculate, with a mixed quantum mechanics/molecular dynamics (QM/MD) theoretical−computational methodology based on the Perturbed Matrix Method (PMM),[26−30] the amide I′ IR spectra of polylysine in its three secondary structure states, and compare the results with the experimental data. The good agreement between the calculated spectra and the experimental spectra enables us to address the following questions: (i) How much can we learn from a model system such as polylysine on the assignment of amide I′ bands to specific secondary-structure elements in proteins? (ii) Are there other factors beyond the excitonic coupling playing a role in the frequency shifts of the amide I′ band as a function of the different secondary-structure states? (iii) What is the effect on the band position and line shape of treating the solvent molecules explicitly compared to an implicit representation based on a mean-field approach?

## THEORY

The methodology used here to reconstruct amide I′ infrared spectra has been explained in detail in previous articles.[26−30] Hereafter, the theoretical basis of PMM calculations and the computational procedure used to obtain vibrational spectra of solvated peptides are briefly outlined.

In PMM calculations,[31−35] similarly to other mixed quantum-classical procedures,[36−38] it is essential to predefine a portion of the system to be treated at electronic level, hereafter termed as quantum center (QC), with the rest of the system described at a classical atomistic level exerting the perturbation on the QC electronic states.

The QC used here to model each peptide group along the peptide backbone is *trans*-*N*-methylamide (NMA). An orthonormal set of unperturbed electronic Hamiltonian ($\tilde{H}^0$) eigenfunctions are initially evaluated on the QC structure of interest (see Methods). Then, after have fitted *trans*-NMA on the given peptide group, the perturbed electronic ground state energy is calculated for each peptide group with the following procedure. Indicating with $V$ and $\boldsymbol{E}$ the perturbing electric potential and field, respectively, exerted by the environment on the QC (typically obtained by the environment atomic charge distribution and evaluated in the QC center of mass), the perturbed electronic Hamiltonian ($\tilde{H}$) for each QC-environment configuration (as generated by the MD simulation) can be constructed:

$$\tilde{H} \simeq \tilde{H}^0 + \tilde{I}q_T V + \tilde{Z}_1 + \Delta V\tilde{I} \tag{1}$$

$$[\tilde{Z}_1]_{j,j'} = -\boldsymbol{E}\cdot\langle\Phi_j^0|\hat{\boldsymbol{\mu}}|\Phi_{j'}^0\rangle \tag{2}$$

where $q_T$, $\hat{\boldsymbol{\mu}}$, and $\Phi_j^0$ are the QC total charge, dipole operator, and unperturbed electronic eigenfunctions, respectively, $\Delta V$ approximates all the higher order terms as a simple short-range potential, $\tilde{I}$ is the identity matrix, and the angled brackets indicate integration over the electronic coordinates. The diagonalization of $\tilde{H}$ provides a set of eigenvectors and eigenvalues representing the QC perturbed electronic eigenstates and energies. Note that the side chain of the considered peptide group, the N-1 residues, and the solvent define the perturbing environment at each configuration generated by the MD simulation. Hence, via a polynomial fit of the perturbed electronic ground state energy along the mode coordinate, the perturbed frequencies for each oscillator along the peptide at each MD frame can be obtained.

The basic approximation of the methodology presented so far is that, for typical quantum vibrational degrees of freedom, the environment perturbation does not significantly alter the vibrational modes (i.e., the mass-weighted QC Hessian eigenvectors) but only the related eigenvalues. Such an assumption provides a good approximation when, under the perturbation, a vibrational mode remains largely uncoupled from the other QC modes as well as from the vibrational modes of the solvent molecules. When modes coupling effects due to interacting vibrational centers ought to be considered, excitonic effects must be included in the calculations.

The perturbed frequencies of the $k$th's chromophore oscillators (here we consider only the amide I′ mode for each chromophore) are thus used to include the excitonic effect by the construction and diagonalization of the excitonic vibronic Hamiltonian matrix (i.e., the vibronic Hamiltonian matrix for the interacting chromophores) given by[28]

$$\tilde{H} = \tilde{I}\mathcal{U}_{\mathrm{vb},0} + \Delta\tilde{H} \tag{3}$$

with $\mathcal{U}_{\mathrm{vb},0}$ the (vibronic) ground state energy of the interacting chromophores and $\Delta\tilde{H}$ the excitation matrix[28] whose diagonal elements are

$$[\Delta\tilde{H}]_{k,k} = h\nu_k \tag{4}$$


dx.doi.org/10.1021/jp211063x | J. Phys. Chem. B XXXX, XXX, XXX−XXX

and whose nonzero off-diagonal elements are given by the chromophores interaction operator (within the dipolar approximation):

$$\hat{V}_{k,k'(k\neq k')} = \frac{\hat{\boldsymbol{\mu}}_k \cdot \hat{\boldsymbol{\mu}}_{k'}}{|\boldsymbol{R}_{k,k'}|^3} - 3\frac{(\hat{\boldsymbol{\mu}}_k \cdot \boldsymbol{R}_{k,k'})(\hat{\boldsymbol{\mu}}_{k'} \cdot \boldsymbol{R}_{k,k'})}{|\boldsymbol{R}_{k,k'}|^5} \quad (5)$$

with $\nu_k$ the $k$th chromophore amide I′ excitation frequency, $\hat{\boldsymbol{\mu}}_k$ the $k$th chromophore dipole operator and $\boldsymbol{R}_{k,k'}$ the $k'$ to $k$ chromophore displacement vector defined by the corresponding chromophores origins. Note that in the present case in the vibronic Hamiltonian matrix for each chromophore only the first vibrational excitation of the electronic ground state must be involved, as higher vibrational excitations are forbidden and the coupling with excited electronic states may be neglected. By diagonalizing the excitation matrix and using the transition dipole for the $0 \rightarrow i$ excitonic transition ($\boldsymbol{\mu}_{0,i}$) as obtained via the excitonic eigenvectors, we may reconstruct the spectral signal of the excitonic system by summing the absorbance due to each $0 \rightarrow i$ transition, providing

$$\varepsilon(\nu) = \sum_i \frac{|\boldsymbol{\mu}_{0,i}|^2 \rho_i(\nu) h\nu}{6\varepsilon_0 c\hbar^2} \quad (6)$$

with $\rho_i$ the probability density in $\nu$ frequency space for the $i$th excitation and $\varepsilon_0$ the vacuum dielectric constant.

## METHODS

**Unperturbed Quantum Chemical Calculations.** As a model of the peptide group, i.e., the quantum center to be explicitly treated at electronic level, *trans*-NMA is chosen. Quantum chemical calculations are carried out on the isolated *trans*-NMA molecule at the time dependent density functional theory (TDDFT) with the 6-31+G(d) basis set. This level of theory is selected because it represents a good compromise between computational costs and accuracy. The mass-weighted Hessian matrix is calculated on the optimized geometry at the B3LYP/6-31+G(d) level of theory and subsequently diagonalized for obtaining the unperturbed eigenvectors and related eigenvalues. The eigenvector corresponding in vacuo to the amide I′ mode is, then, used to generate a grid of points (i.e., configurations) as follows: a step of 0.05 au is adopted, and the number of points is set to span an energy range of 20 kJ/mol (in the present case 31 points). For each point, six unperturbed electronic states are then evaluated at the same level of theory providing the basis set for the PMM calculations.

**Molecular Dynamics Simulations.** The initial structures of the $\alpha$-helix and $\beta$-sheet conformations of polylysine were modeled with the program Molden 3.8[39] starting from secondary structure models based on hydrogen bonds patterns and backbone dihedral angles. The 20-residue helical conformation and the antiparallel $\beta$-sheet made up of 6-strands each containing 7 lysine residues (shown in Figure 1, panels A and B, respectively) were placed in a periodic dodecahedral box large enough to contain the peptide and 1.0 nm of solvent ($D_2O$) on all sides. Water was modeled using the deuterated simple point charge (SPC) water model.[40] The 15-stranded $\beta$-sheet conformation was obtained by adding the necessary number of strands to the 6-stranded sheet in the antiparallel arrangement and was then solvated in a conveniently bigger box. Optimization of the solvated structures was done by using the empirical potential energy function of the GROMOS96 43a1 force field.[41] In order to reproduce the experimental conditions (pH = 12), lysine side chains were not protonated.

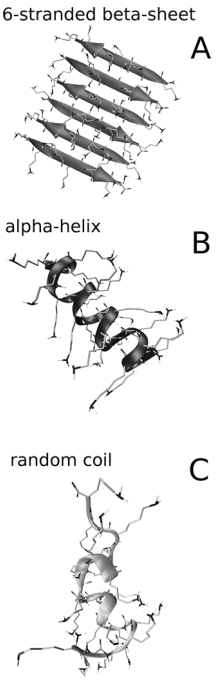


**Figure 1.** Representative structures of polylysine in the three different secondary-structure states. Panel A: 6-stranded $\beta$-sheet conformation (each strand is made up of 7 residues); panel B: 20-residue $\alpha$-helix conformation; panel C: 20-residue random coil conformation.

One 40 ns long MD simulation of each of the three structures was performed after energy minimization in explicit solvent in the NVT ensemble, with fixed bond lengths[42] with the GROMACS software package[43] and with the GROMOS96 43a1 force field. A nonbonded pairlist cutoff of 9.0 Å was used, periodic boundary conditions were used, and the long-range electrostatic interactions were treated with the particle mesh Ewald method.[44] The isokinetic temperature coupling[45] was used to keep the temperature constant at 300 K. The initial secondary structures are well retained during the simulations.

The random coil conformation, experimentally obtained at low pH, was here obtained by performing a high-temperature (500 K) MD simulation starting from the $\alpha$-helix conformation. High temperature, rather than low pH, was here chosen for the random coil simulation in order to avoid changing the protonation state of the lysine side chains with respect to the $\alpha$-helix and $\beta$-sheet systems. After a 10 ns long equilibration run, necessary to the system to completely lose the helical structure, a 20 ns long MD simulation at 500 K was performed using the same simulation protocol described above. A representative snapshot extracted from this simulation is shown in Figure 1, panel C.

Note that, in order to fit *trans*-NMA to the peptide group of each residue (see Theory), the first and last residue of the $\alpha$-helix and of the random coil conformations and the first and last residue of each strand of the two $\beta$-sheet conformations were not used in the PMM calculations. The total number of residues participating to the PMM calculations were thus 18 for the helix and the random coil secondary structure, 30 for the 6-stranded $\beta$-sheet, and 75 for the 15-stranded $\beta$-sheet.


dx.doi.org/10.1021/jp211063x | J. Phys. Chem. B XXXX, XXX, XXX–XXX

## RESULTS AND DISCUSSION

Amide I′ spectra of polylysine peptides in different conformations ($\beta$-sheet, $\alpha$-helix, and random coil) have been experimentally characterized,[4] showing secondary structure sensitivity of the absorption bands. Indeed, the $\alpha$-helix amide I′ peak is centered at ≈1634 cm$^{-1}$, the $\beta$-sheet structure is characterized by a main peak red-shifted by ≈24 cm$^{-1}$ with respect to the helix peak and a smaller peak at ≈1680 cm$^{-1}$, and the random coil absorption peak is blue-shifted by ≈10 cm$^{-1}$ with respect to the helix peak. It is worth to note that in such experimental studies no explicit information on the size of the polylysine secondary structure is available, and probably, the experimental spectroscopic signal is due to a mixed population of secondary structures of different dimensions.

The amide I′ spectra of a polylysine peptide in its three secondary structure conformations (6-stranded $\beta$-sheet, $\alpha$-helix, and random coil) were here calculated by using the PMM/MD methodology explained in the Theory section. The spectra were calculated both using the full procedure, i.e., including the excitonic coupling (Figure 2A), and without the inclusion of the excitonic coupling (Figure 2B). In Figure 2D are shown, for comparison, the experimental spectra.[4] The computed spectra were shifted to lower frequencies by ≈75 cm$^{-1}$ in order to align the peak of the $\alpha$-helix conformation with the corresponding experimental one. Such a shift, largely due to the inaccuracies of the *ab initio* calculations, was applied to all the computed spectra of the polylysine peptides. Comparison of the spectra in panels A and B of Figure 2 shows that the relative frequency shift due to the change of the secondary structure is reproduced also in the absence of the excitonic coupling. This result points to a role played by the environment perturbation on the amide I′ relative frequency shifts beyond the widely accepted effect of the excitonic coupling.[26,28]

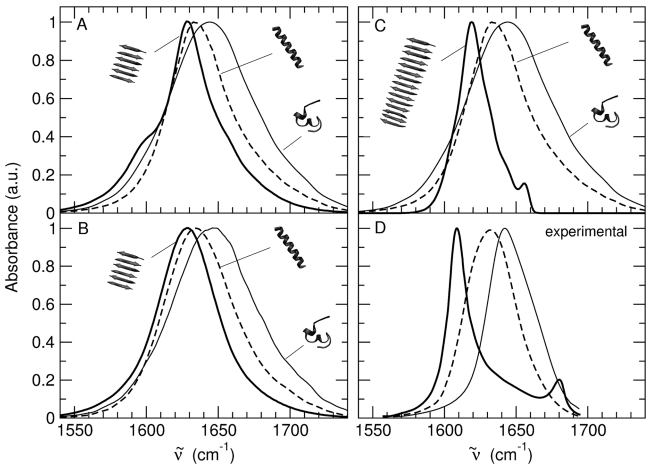


**Figure 2.** Amide I′ spectra of the polylysine peptide in $D_2O$ in three different secondary structural states: random coil (solid thin line), $\alpha$-helix (dashed line), and $\beta$-sheet (solid thick line). (A) Calculated spectra with the inclusion of the excitonic coupling; the $\beta$ conformation is a 6-stranded $\beta$-sheet. (B) Calculated spectra without the inclusion of the excitonic coupling; the $\beta$ conformation is a 6-stranded $\beta$-sheet. (C) Calculated spectra with the inclusion of the excitonic coupling; the $\beta$ conformation is a 15-stranded $\beta$-sheet. (D) Experimental spectra. The height of each spectrum has been normalized to 1.

While the shift between the helix and the random coil conformations is quantitatively reproduced, being ≈12 cm$^{-1}$ vs the experimental ≈10 cm$^{-1}$, the shift between the $\beta$-sheet peak and the $\alpha$-helix peak is rather underestimated, being ≈6 cm$^{-1}$ vs the experimental ≈24 cm$^{-1}$. The addition of the excitonic coupling to the calculation (Figure 2, panel A) does not affect the relative position of the main peaks (only the random coil peak is slightly red-shifted by 3 cm$^{-1}$) but results in an evident narrowing of the $\beta$-sheet absorption band, in line with the experiments showing that the $\beta$-sheet amide I′ band is narrower than the others. However, the full width at half-maximum (fwhm) of the calculated spectrum is still larger than the experimental one (38 cm$^{-1}$ vs 14 cm$^{-1}$), a shoulder can be seen on the left of the computed band that is not present in the experimental spectrum and the splitting of the band into an intense, main peak and a secondary, high frequency peak observed in the experiments is missing. It should also be noted that the fwhm of the computed random coil peak is larger than the experimental fwhm. This is most probably due to the high temperature used in the random coil simulation (500 K vs the experimental temperature of 300 K) and to the infinite dilution condition used in the simulation, while in the experiments a mixture of variously sized aggregates is expected to be present.

In what follows the effect of larger $\beta$-sheet structures on the band shape and position is investigated by calculating the amide I′ band of a 15-stranded $\beta$-sheet and of an aggregate made up of 3 sheets each containing 15 strands. The two spectra, shown in Figure 3, are very similar. When the larger $\beta$-sheet systems are considered, the agreement between the calculated and the experimental spectra clearly improves (see Figure 2, panels C and D): (i) the spectra of the larger $\beta$-structures become indeed red-shifted by ≈10 cm$^{-1}$ with respect to the 6-stranded $\beta$-sheet spectrum (see Figure 3), resulting in a overall shift of 16 cm$^{-1}$ from the $\alpha$-helix peak vs the experimental 24 cm$^{-1}$; (ii) the fwhm is better reproduced (24 and 18 cm$^{-1}$ for the single-sheet and the aggregate, respectively, vs the experimental 14 cm$^{-1}$), and the shoulder observed on the left of the 6-stranded $\beta$-sheet spectrum disappears (see Figure 3); (iii) in the spectra of the larger $\beta$-structures the secondary peak at high frequency, that is due to excitonic coupling and was missing in the 6-stranded sheet, is now present (see Figure 3); the shift between the main and the secondary peak is ≈36 cm$^{-1}$ vs the experimental ≈70 cm$^{-1}$.

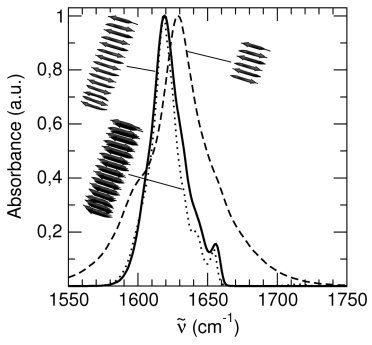


**Figure 3.** Calculated amide I′ spectra of the polylysine peptide in $D_2O$ in three $\beta$-sheet conformations: one sheet made up of 6 strands (dashed line), one sheet made up of 15 strands (solid line), and three sheets each made up of 15 strands (dotted line). The height of each spectrum has been normalized to 1. The full PMM procedure (i.e., with the inclusion of the excitonic coupling) was used.

From the comparison between the spectra of the shorter and longer $\beta$-sheet (Figure 3) it emerges that the number of strands


dx.doi.org/10.1021/jp211063x | J. Phys. Chem. B XXXX, XXX, XXX–XXX

that constitutes the polylysine peptide affects the position of the main peak, in agreement with previous experimental observations that proved that sheets with a larger number of strands have a lower spectral position of the main band.[3] Also, the frequency difference between the main and the secondary peak was shown, in previous work, to be a function of the number of participating strands;[29,46,47] i.e., the longer the sheet, the larger the peak-to-peak distance. Although the frequency difference for the 15-stranded sheet calculated in the present work is lower (≈36 $cm^{-1}$) than the experimental value (≈70 $cm^{-1}$), we expect to get closer to the experimental ≈70 $cm^{-1}$ by increasing the length of the sheet. Nevertheless, it cannot be excluded that also the approximations used in our calculations, i.e., modes coupling is modeled only via excitonic effects treated within the dipolar approximation, may affect the accuracy of our estimate of the frequency shift.

From the above data, and from previous studies,[48−50] the spectral features usually assigned to a generic $\beta$-sheet conformation, i.e., a main band at low frequency (≈1620 $cm^{-1}$) and the splitting of the amide I′ band into two peaks, seem to correspond, instead, to sufficiently organized and extended $\beta$-sheets, which are rare in native proteins. In fact, in the amide I′ spectra of common globular proteins the high-frequency peak reduces to a shoulder,[25] with the exception of $\beta$-barrels that show, indeed, a splitted amide I′ band.[51]

Extended $\beta$-structures with a large number of consecutive strands as the ones just discussed are more representative of aggregates and/or amyloids. In fact, the splitting of the amide I′ spectrum into two bands centered around 1610−1620 and 1680 $cm^{-1}$ is often observed in the spectra of peptides and proteins that form amyloid aggregates (more interacting sheets).[48−50,52−56] Experimental evidence of this can be found in various systems. For example, Zurdo et al.[48] observed the splitting of the amide I′ band of the fibril-forming SH3 domain of the $\alpha$-subunit of bovine phosphatidylinositol-3′-kinase only at long incubation times, while it is known that also the monomer contains two sets of antiparallel $\beta$-sheets of three and two strands.[57] Janek et al.,[49] studying a series of water-soluble $\beta$-sheet peptides [DPKGDPKG-(VT)$n$-GKGDPKPD-NH2, $n$ = 3−8], associated the double-peaked IR spectra with the formation of big water-soluble peptide complexes. Zandomeneghi et al.[50] stated that native $\beta$-sheet proteins and amyloid fibrils differ in the amide I′ band, observing the sharp double-peaked spectrum only in the presence of amyloid fibrils.

Remarkably, the hypothesis that the appearance of an intense band and a higher energy band is the typical spectral pattern associated with antiparallel $\beta$-sheet aggregates, rather than to a generic antiparallel $\beta$-sheet structure, was already proposed some years ago[58−62] but has met with little success. In particular, concerning polylysine, Jackson et al.[61] proposed that the $\beta$-sheet conformation of polylysine is, rather than a typical $\beta$-sheet structure, "more likely to consist of extended strands of polylysine stabilized by intermolecular hydrogen bonds".[61]

In order to investigate the solvent effects on the amide I′ band shape of the $\beta$-sheet conformation, the spectra corresponding to the 15-stranded and the 6-stranded $\beta$-sheets of the polylysine peptide were reconstructed in vacuum, i.e. without considering the solvent as part of the perturbing environment during the PMM calculation (see Theory section). The vacuum spectra of the 15-stranded and the 6-stranded $\beta$-sheet, presented in Figure 4, are very similar, showing the splitting of the band into two peaks. On the contrary, when the electric field exerted by the water molecules is included in the

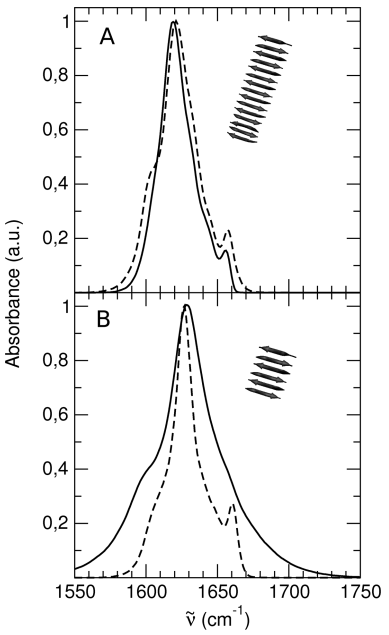


**Figure 4.** Computed amide I′ spectra of the polylysine peptide in the 15-stranded $\beta$-sheet conformation (panel A) and in the 6-stranded $\beta$-sheet conformation (panel B). The spectra in each panel correspond to the same structure in vacuum (dashed line) and in $D_2O$ solution (solid line). The height of each spectrum has been normalized to 1. The full PMM procedure (i.e., with the inclusion of the excitonic coupling) was used.

calculation, the two conformations give different results: in the case of the 15-stranded sheet (Figure 4, panel A) the addition of the solvent does not change the spectrum while in the case of the 6-stranded sheet (Figure 4, panel B) the secondary peak disappears and the bandwidth increases. This result points to a crucial role of the aqueous solvent on the spectral shape of the amide I′ band of $\beta$-sheets.

The origin of the differences between the spectra of the two sheets was further investigated by analyzing the single-residue spectra of each amino acid (i.e., as obtained by the distribution of the single-residue perturbed frequencies along the MD trajectory, hence without considering any excitonic coupling). The single-residue spectra of the 15-stranded sheet have similar bandwidths, while the single-residue spectra of the 6-stranded sheet show a much higher bandwidth variability. This can be observed in Figure 5, in which the value of the standard deviation of the spectrum of each residue of the 15-stranded sheet (panel A, solid line) and of the 6-stranded sheet (panel B, solid line) is reported as a function of the residue index (similar results were obtained when considering one of the three 15-stranded sheet of the aggregate). The standard deviations of the 30 residues of the 6-stranded sheet are distributed in the range between 13.3 and 43.4 $cm^{-1}$ with a mean value of 25.3 $cm^{-1}$, while the standard deviations of the 75 residues of the 15-stranded sheet are distributed in the range between 5.6 and 13.6 $cm^{-1}$ with a mean value of 8.9 $cm^{-1}$. Moreover, it can be seen from Figure 5 (panel B, dotted line) that the larger variability of the single residue spectra of the 6-stranded sheet mainly depends on the solvent contribution, thus confirming the importance of the role of the solvent. This means that, because of the solvent contribution, the instantaneous frequencies of each residue are much more variable in the smaller system than in the bigger one. This variability leads to


dx.doi.org/10.1021/jp211063x | J. Phys. Chem. B XXXX, XXX, XXX−XXX

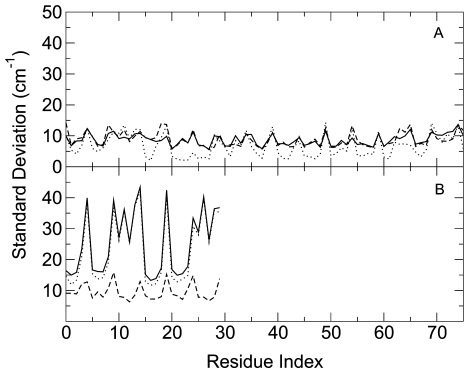


**Figure 5.** Values of the standard deviations of the single-residue spectra of the 15-stranded sheet (panel A) and of the 6-stranded sheet (panel B). In each panel the values of the standard deviations of the single residue spectra are calculated considering as perturbing environment only the solvent (dotted line) only the peptide (dashed line) and both the solvent and the peptide (solid line).

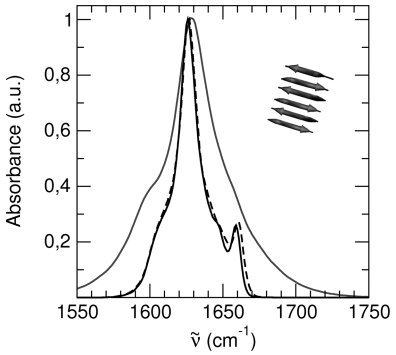


**Figure 6.** Computed amide I′ spectra of the polylysine peptide in the 6-stranded $\beta$-sheet conformation in vacuum (dashed line) in $D_2O$ solution (solid gray line) and considering the solvent effect as a constant field effect (solid black line). The height of each spectrum has been normalized to 1. The full PMM procedure (i.e., with the inclusion of the excitonic coupling) was used.

the disappearance of the high frequency peak because of a 2-fold effect: a weaker excitonic coupling and the broadening of the main peak to such an extent that the excitonic peak is convolved within the main peak. In the bigger sheet (Figure 5A), the fluctuations of the solvent perturbing effect, even though slightly larger than the ones of the peptide perturbing effect, are considerably smaller if compared to the corresponding fluctuations in the 6-stranded sheet, leading to an overall smaller variability.

The previously mentioned crucial role of the aqueous solvent seems thus to reside in the fluctuations of the solvent perturbing effect that gives rise to the broader band observed for the 6-stranded sheet. In other words, the splitting of the amide I′ band into two peaks also occurs in smaller $\beta$-sheet structures (e.g., a 6-stranded sheet) but becomes actually visible (at least in a solvent like water) only when the $\beta$-structure is sufficiently extended and well-organized, with strong intrasheet or intersheet interactions. This sufficient organization is likely to correspond to some kind of aggregation (e.g., $\beta$-barrels, amyloid aggregates).

The importance of the fluctuations of the solvent was confirmed by the calculation of the spectrum of the 6-stranded sheet considering the perturbing effect of the solvent as a constant field effect. The constant field effect was calculated as follows. For each residue, at every frame of the simulated trajectory, the difference between the frequency obtained by considering both the solvent and the peptide as perturbing environment and the frequency calculated in vacuum was calculated. The mean value of such differences was, then, added to the vacuum frequencies as constant field effect (note that for every residue a different constant field effect was obtained). The results of the calculation are reported in Figure 6, showing a spectrum very similar to the vacuum one. Neglecting the time variability of the solvent perturbation leads to a very different shape of the amide I′ band and seems, thus, an inaccurate approximation at least for small sheets (6-stranded in the present case).

The use of a constant field effect to treat the solvent in IR spectra calculations seems a reasonable approximation in the case of extended systems. On the contrary, the use of this approximation in the case of small $\beta$-sheets or even $\beta$-hairpins might lead to inaccurate spectral shapes providing, for example, a double-peak amide I′ signal rather than a single, broader band. Hence, as previously proposed,[58−62] and further strengthen here, the presence of the high-frequency minor peak in the amide I′ spectrum more likely represents some kind of $\beta$-aggregates.

## CONCLUSIONS

Infrared spectroscopy is widely used to understand the conformation of peptides and proteins in solution (i.e., folded or unfolded state) and to obtain information about their secondary structure. The amide I′ band of peptides and proteins is indeed secondary-structure sensitive, but it is well-known that the assignment of specific spectral features to one secondary structure state is very difficult and often ambiguous, and it is easy to find different frequency assignments to the same secondary structure. Polylysine peptides specifically designed at the purpose have been used as benchmark systems to assign spectral features to specific secondary structures. However, according to our results, the experimental solution conditions supposed to provide the spectrum of a generic $\beta$-sheet structure lead instead to the formation of soluble aggregates. By calculating the spectra of polylysine in various $\beta$-sheet conformations, we showed indeed that the sharp double-peaked amide I′ band assigned to the antiparallel $\beta$-sheet, rather well corresponds to sufficiently well-organized and extended $\beta$-structures in which strong intra- and/or intersheet interactions are present. This conditions are likely to correspond in solution to the formation of aggregates. Usually, in the experiments a broad population of variously sized oligomers and aggregates is expected to be present (particularly for peptides). While according to our results it could be possible to distinguish between extended and short $\beta$-sheets, it seems difficult for short peptides to distinguish between $\alpha$- and $\beta$-structures as the corresponding amide I′ signals largely overlap.

We also demonstrated that the solvent has a crucial role in the shape determination of the amide I′ band of $\beta$-sheet conformations and in particular in the disappearance of the high-frequency secondary peak for small $\beta$-sheets. We showed indeed that, if the $\beta$-structure is not sufficiently extended, the time fluctuations of the perturbing effect of the solvent give rise to a weaker excitonic coupling and to a broad band in which both the main peak and the high-frequency peak are convolved.

The role of the excitonic coupling on the amide I′ frequency position as a function of the secondary-structure state was also addressed. The comparison of the spectra calculated with and


dx.doi.org/10.1021/jp211063x | J. Phys. Chem. B XXXX, XXX, XXX−XXX

without the inclusion of the excitonic coupling showed that secondary-structure sensitive frequency shifts do not uniquely depend on the coupling effects and that the excitonic coupling influences mainly the spectral shape.

## AUTHOR INFORMATION


### Corresponding Author

*E-mail: daidone@caspur.it (I.D.); andrea.amadei@uniroma2.it (A.A.).


### Notes

The authors declare no competing financial interest.

## ACKNOWLEDGMENTS

We acknowledge CASPUR (Consorzio interuniversitario per le Applicazioni di Supercalcolo Per Università e Ricerca) for the use of a its computational facilities and its financial support with the project "Theoretical study of electron transfer reactions in complex atomic-molecular systems".

## REFERENCES


(1) Surewicz, W. K.; Mantsch, J. H. H.; Chapman, D. *Biochemistry* **1993**, *32*, 389−394.
(2) Kumosinski, T. F.; Unruh, J. J. *Talanta* **1996**, *43*, 199−219.
(3) Barth, A. *Biochim. Biophys. Acta* **2007**, *1767*, 1073−1101.
(4) DeFlores, L. P.; Ganim, Z.; Nicodemus, R. A.; Tokmakoff, A. *J. Am. Chem. Soc.* **2009**, *131*, 3385−3391.
(5) Smith, A. W.; Tokmakoff, A. *J. Chem. Phys.* **2007**, *126*, 45109−11.
(6) Smith, A. W.; Chung, H. S.; Ganim, Z.; Tokmakoff, A. *J. Phys. Chem. B* **2005**, *109*, 17025−17027.
(7) Arrondo, J. L. R.; Blanco, F. J.; Serrano, L.; Goñi, F. M. *FEBS Lett.* **1996**, *384*, 35−37.
(8) Hilario, J.; Kubelka, J.; Keiderling, T. A. *J. Am. Chem. Soc.* **2003**, *125*, 7562−7574.
(9) Kwac, K.; Cho, M. *J. Chem. Phys.* **2003**, *119*, 2247−2255.
(10) Schmidt, J. R.; Corcelli, S. A.; Skinner, J. L. *J. Chem. Phys.* **2004**, *121*, 8887−8896.
(11) Gaigeot, M. P.; Vuilleumier, R.; Sprik, M.; Borgis, D. *J. Chem. Theory Comput.* **2005**, *1*, 772−789.
(12) Gorbunov, R. D.; Nguyen, P. H.; Kobus, M.; Stock, G. *J. Chem. Phys.* **2007**, *126*, 054509−054518.
(13) Krimm, S.; Bandekar, J. *Adv. Protein Chem.* **1986**, *38*, 181−364.
(14) Torii, H.; Tasumi, M. *J. Chem. Phys.* **1992**, *96*, 3379−3387.
(15) Lee, S. H.; Krimm, S. *Biopolymers* **1998**, *46*, 283−317.
(16) Moran, A.; Mukamel, S. *Proc. Natl. Acad. Sci. U. S. A.* **2004**, *101*, 506−510.
(17) Brauner, J. W.; Flach, C. R.; Mendelsohn, R. *J. Am. Chem. Soc.* **2005**, *127*, 100−109.
(18) Yang, S.; Cho, M. *J. Chem. Phys.* **2005**, *123*, 134503−134505.
(19) Bour, P.; Keiderling, T. A. *J. Phys. Chem. B* **2005**, *109*, 23687−23697.
(20) Ham, S.; Cha, S.; Choi, J. H.; Cho, M. *J. Chem. Phys.* **2003**, *119*, 1451−1462.
(21) Hahn, S.; Ham, S.; Cho, M. *J. Phys. Chem. B* **2005**, *109*, 11789−11801.
(22) Choi, J. H.; Lee, H.; Lee, K. K.; Hahn, S.; Cho, M. *J. Chem. Phys.* **2007**, *126*, 045102−045116.
(23) Jackson, M.; Haris, P. I.; Chapman, D. *Biochim. Biophys. Acta* **1989**, *998*, 75−79.
(24) Carrier, D.; Mantsch, H. H.; Wong, P. T. T. *Biopolymers* **1990**, *29*, 837−844.
(25) Ganim, Z.; Chung, H. S.; Smith, A. W.; DeFlores, L. P.; Jones, K. C.; Tokmakoff, A. *Acc. Chem. Res.* **2008**, *41*, 432−441.
(26) Daidone, I.; Aschi, M.; Zanetti-Polzi, L.; Di Nola, A.; Amadei, A. *Chem. Phys. Lett.* **2010**, *488*, 213−218.
(27) Amadei, A.; Daidone, I.; Di Nola, A.; Aschi, M. *Curr. Opin. Struct. Biol.* **2010**, *20*, 155−161.
(28) Amadei, A.; Daidone, I.; Zanetti-Polzi, L.; Aschi, M. *Theor. Chem. Acc.* **2011**, *129*, 31−43.
(29) Zanetti-Polzi, L.; Amadei, A.; Aschi, M.; Daidone, I. *J. Am. Chem. Soc.* **2011**, *133*, 11414−11417.
(30) Zanetti-Polzi, L.; Daidone, I.; Anselmi, M.; Carchini, G.; Di Nola, A.; Amadei, A. *J. Phys. Chem. B* **2011**, *115*, 11872−11878.
(31) Aschi, M.; Spezia, R.; Di Nola, A.; Amadei, A. *Chem. Phys. Lett.* **2001**, *344*, 374−380.
(32) Spezia, R.; Aschi, M.; Di Nola, A.; Amadei, A. *Chem. Phys. Lett.* **2002**, *365*, 450−456.
(33) Amadei, A.; D'Abramo, M.; Zazza, C.; Aschi, M. *Chem. Phys. Lett.* **2003**, *381*, 187−193.
(34) Amadei, A.; Marinelli, F.; D'Abramo, M.; D'Alessandro, M.; Anselmi, M.; Di Nola, A.; Aschi, M. *J. Chem. Phys.* **2005**, *122*, 124506−124515.
(35) Amadei, A.; D'Alessandro, M.; D'Abramo, M.; Aschi, M. *J. Chem. Phys.* **2009**, *130*, 084109−084118.
(36) Gao, J.; Truhlar, D. G. *Annu. Rev. Phys. Chem.* **2002**, *53*, 467−505.
(37) Vreven, T.; Morokuma, K. *Annu. Rep. Comput. Chem.* **2006**, *2*, 35−52.
(38) Senn, H. M.; Thiel, W. *Curr. Opin. Chem. Biol.* **2007**, *11*, 182−187.
(39) Schaftenaar, G.; Noordik, J. *J. Comput.-Aided Mol. Des.* **2000**, *14*, 123.
(40) Berendsen, H. J. C.; Grigera, J. R.; Straatsma, T. P. *J. Phys. Chem.* **1987**, *91*, 6269−6271.
(41) van Gunsteren, W. F.; Billeter, S.; Eising, A.; Hunenberg, P.; Kruger, P.; Mark, A. E.; Scott, W.; Tironi, I. *Biomolecular Simulations: The GROMOS96 Manual and User Guide*; Hochschulverlag an der ETH Zurich: Zurich, 1996.
(42) Hess, B.; Bekker, H.; Berendsen, H. J. C.; Fraaije, J. G. E. M. *J. Comput. Chem.* **1997**, *18*, 1463−1472.
(43) Berendsen, H. J. C.; van der Spoel, D.; van Drunen, R. *Comput. Phys. Commun.* **1995**, *91*, 43−56.
(44) Darden, T.; York, D.; Pedersen, L. *J. Chem. Phys.* **1993**, *98*, 10089−10092.
(45) Brown, D.; Clarke, J. H. R. *Mol. Phys.* **1984**, *51*, 1243−1252.
(46) Hahn, S.; Kim, S.; Lee, C.; Cho, M. *J. Chem. Phys.* **2005**, *123*, 084905−084914.
(47) Cheatum, C.; Tokmakoff, A.; Knoester, J. *J. Chem. Phys.* **2004**, *120*, 8201−8215.
(48) Zurdo, J.; Guijarro, J. I.; Jimenez, J. L.; Saibil, H. R.; Dobson, C. M. *J. Mol. Biol.* **2001**, *311*, 325−340.
(49) Janek, K.; Behlke, J.; Zipper, J.; Fabian, H.; Georgalis, Y.; Beyermann, M.; Bienert, M.; Krause, E. *Biochemistry* **1999**, *38*, 8246−8252.
(50) Zandomeneghi, G.; Krebs, M.; McCammon, M.; Fändrich, M. *Protein Sci.* **2004**, *13*, 3314−3321.
(51) Lefèvre, T.; Subirade, M. *Int. J. Biol. Macromol.* **2000**, *28*, 59−67.
(52) Yamada, N.; Ariga, K.; Naito, M.; Matsubara, K.; Koyama, E. *J. Am. Chem. Soc.* **1998**, *120*, 12192−12199.
(53) Silva, R. A. G. D.; Barber-Armstrong, W.; Decatur, S. M. *J. Am. Chem. Soc.* **2003**, *125*, 13674−13675.
(54) Petty, S. A.; Decatur, S. M. *Proc. Natl. Acad. Sci. U. S. A.* **2005**, *102*, 14272−14277.
(55) Petty, S. A.; Adalsteinsson, T.; Decatur, S. M. *Biochemistry* **2005**, *44*, 4720−4726.
(56) Castelletto, V.; Hamley, I.; Harris, P. *Biophys. Chem.* **2008**, *138*, 29−35.
(57) Bader, R.; Bamford, R.; Zurdo, J.; Luisi, B. F.; Dobson, C. M. *J. Mol. Biol.* **2005**, *356*, 189−208.
(58) Dong, A.; Matsuura, J.; Manning, M. C.; Carpenter, J. F. *Arch. Biochem. Biophys.* **1998**, *355*, 275−281.
(59) Panick, G.; Malessa, R.; Winter, R. *Biochemistry* **1999**, *38*, 6512−6519.
(60) Parris, N.; M. P., S.; Purcell, J. M. *J. Agric. Food Chem.* **1991**, *39*, 2167−2170.

(61) Jackson, M.; Mantsch, H. H. *Crit. Rev. Biochem. Mol. Biol.* **1995**, *30*, 95−120.
(62) Kubelka, J.; Keiderling, T. A. *J. Am. Chem. Soc.* **2001**, *123*, 12048−12058.